Energy Crisis in the Superbubble DEM L 192 (N 51D)

Randall L. Cooper[1,2], Martín A. Guerrero[1,3], You-Hua Chu[1], C.-H. Rosie Chen[1], Bryan C. Dunne[1]

Astronomy Department, University of Illinois, 1002 West Green Street, Urbana, IL 61801

ABSTRACT

Superbubbles surrounding OB associations provide ideal laboratories to study the stellar energy feedback problem because the stellar energy input can be estimated from the observed stellar content of the OB associations and the interstellar thermal and kinetic energies of superbubbles are well-defined and easy to observe. We have used DEM L 192, also known as N 51D, to carry out a detailed case study of the energy budget in a superbubble, and we find that the expected amount of stellar mechanical energy injected into the ISM, $(18 \pm 5) \times 10^{51}$ ergs, exceeds the amount of thermal and kinetic energies stored in the superbubble, $(6 \pm 2) \times 10^{51}$ ergs. Clearly, a significant fraction of the stellar mechanical energy must have been converted to other forms of energy. The X-ray spectrum of the diffuse emission from DEM L 192 requires a power-law component to explain the featureless emission at 1.0–3.0 keV. The origin of this power-law component is unclear, but it may be responsible for the discrepancy between the stellar energy input and the observed interstellar energy in DEM L 192.

Subject headings: ISM: bubbles — ISM: individual (DEM L 192) – Stars: winds, outflows – Supernovae: general – X-ray: ISM

1. Introduction

Massive stars inject large amounts of mechanical energy into the ambient interstellar medium (ISM) via fast stellar winds and supernova explosions. The stellar energy feedback

[1]Astronomy Department, University of Illinois, 1002 W. Green Street, Urbana, IL 61801; rcooper1@astro.uiuc.edu, mar@astro.uiuc.edu, chu@astro.uiuc.edu c-chen@astro.uiuc.edu, carolan@astro.uiuc.edu

[2]Now at Department of Astronomy, Harvard University, rcooper@cfa.harvard.edu

[3]Now at Instituto de Astrofísica de Andalucía (CSIC), Spain.

alters the physical conditions of the ISM and consequently may regulate the formation of future-generation stars. To gain a better understanding of the physical structure and evolution of the ISM in a galaxy, it is necessary to investigate empirically the conversion efficiency of stellar mechanical energies into interstellar kinetic and thermal energies.

Massive stars usually form in groups such as OB associations, and their fast stellar winds and supernova ejecta collectively sweep up the ambient ISM to form superbubbles (Mac Low & McCray 1988). Superbubbles provide excellent laboratories to study the effects of stellar energy feedback on the ISM because the kinetic and thermal energies in a superbubble are well-defined and can be measured with little ambiguity. Superbubbles in the Large Magellanic Cloud (LMC) at 50 kpc are particularly well suited for such studies, as their stellar content and ISM can be observed in great detail with little foreground extinction.

We have chosen the superbubble DEM L 192 (Davies, Elliott, & Meaburn 1976) in the LMC for a detailed study of the interaction between its stars and the ambient ISM. DEM L 192, also known as N 51D (Henize 1956), hosts two OB associations, LH 51 and LH 54 (Lucke & Hodge 1970). The stellar content of these two OB associations and the dynamics of the superbubble have been analyzed in detail by Oey (1996a) and Oey & Smedley (1998). They conclude that LH 51 and LH 54 are both young, $\sim 3 \times 10^6$ yr old. The diffuse X-ray emission from the hot interior of DEM L 192 was detected by *Einstein* and *ROSAT* observations (Chu & Mac Low 1990; Dunne, Points, & Chu 2001), but high-quality spectra of the X-ray emission have been provided only by *XMM-Newton* observations. The emission line features in the X-ray spectra suggest an overabundance in oxygen and neon which is used to argue for the occurrence of supernova explosions (Bomans et al. 2002).

This paper reports our investigation of the energetics of the superbubble DEM L 192. In §2 we analyze archival *XMM-Newton* observations of DEM L 192 to determine the physical properties of the hot gas in the superbubble interior. In §3 we determine the thermal energy of the hot superbubble interior and the kinetic energies of the ionized and neutral gas in the superbubble shell. In §4 we compute the stellar wind energy and supernova explosion energy expected from the known stellar content of LH 51 and LH 54. Finally, a discussion of the overall energy budget of the DEM L 192 superbubble and our conclusions are given in §5.

2. XMM-Newton Observations of Hot Gas in DEM L 192

DEM L 192 was observed with the *XMM-Newton Observatory* on 2001 October 31 and November 1 using the EPIC/MOS1, EPIC/MOS2, and EPIC/pn CCD cameras (Obs. ID: 7194). The two EPIC/MOS cameras were operated in the Prime Full-Window Mode for a

useful exposure time of 31.6 ks, and the EPIC/pn camera was operated in the Extended Prime Full-Window Mode for a useful exposure time of 24.6 ks. The thin filter was used for all observations.

We retrieved the *XMM-Newton* pipeline products from the *XMM-Newton* Science Archive (XSA)[4] and further processed the data using the *XMM-Newton* Science Analysis Software (SAS ver. 5.3.3) and the calibration files from the Calibration Access Layer available on 2002 December 13. The event files were screened to eliminate bad events (e.g., events due to charged particles) so that only events with CCD patterns 0-12 (similar to *ASCA* grades 0-4) were selected for the EPIC/MOS observations, and events with CCD pattern 0 (single pixel events) were selected for the EPIC/pn observation. We also screened the event files to remove periods of high background. To assess the background rate, we binned the counts over 50 s time intervals for each instrument in the 10-12 keV energy range which is dominated by the background. Only for a short period of time did the high background, with count rates $\geq$0.3 counts s^{-1} for the EPIC/MOS or $\geq$0.6 counts s^{-1} for the EPIC/pn, affect the observations; events from this high-background period were discarded. The resulting net exposure times are 30.6 ks and 23.2 ks for the EPIC/MOS and EPIC/pn observations, respectively.

2.1. Spatial Analysis

We extracted images from the EPIC/pn and EPIC/MOS observations in the 0.25–2.5 keV energy band, which includes most of the diffuse X-ray emission from DEM L 192. These images were then combined to obtain a higher S/N ratio image and to reduce the null exposure in the gaps between CCDs (the satellite was not dithered during the observations). The resulting raw EPIC image is presented in Fig. 1a. This image was further adaptively smoothed using Gaussian profiles with FWHM ranging from 2″ to 15″ and divided by a normalized exposure map to remove the vignetting of the telescope and sensitivity variations of the instruments. A grey-scale presentation of this adaptively smoothed EPIC image is shown in Fig. 1b. For comparisons, an Hα image of the same region is displayed in Fig. 1c, and the X-ray contours extracted from the smoothed EPIC image are overplotted on the Hα image in Fig. 1d.

Diffuse X-ray emission from the interior of DEM L 192 is clearly detected. The brightest X-ray emission region is coincident with the OB association LH 54, peaking particularly at

[4]The *XMM-Newton* Science Archive is supported by ESA and can be accessed at http://xmm.vilspa.esa.es/xsa.

the bright Wolf-Rayet star HD 36402. The X-ray peaks coincident with bright stars may be dominated by stellar emission; therefore, emission from these peaks is excluded from our analysis of diffuse X-rays. The diffuse X-ray emission shows a rough limb-brightened morphology in the main body of the superbubble, with the brightest diffuse X-ray emission projected interior to the brightest Hα emission regions of the shell. Faint diffuse X-ray emission is detected to the north and southwest of the main body; however, these faint X-ray extensions do not necessarily imply blowouts, as they are bounded by faint Hα filaments externally. The superbubble DEM L 192 must be in an inhomogeneous ISM, and the variations in the Hα surface brightness reflect the density variations in the ambient ISM. The rough correspondence between the diffuse X-ray surface brightness and the nebular Hα surface brightness suggests that a mixing of the dense, cooler, superbubble shell gas into the hot interior has occurred.

2.2. Spectral Analysis

The X-ray spectrum of DEM L 192 is extracted from only the event file of the EPIC/pn camera because its sensitivity is greater than that of the EPIC/MOS cameras. The source aperture, marked in Fig. 1a, includes a large elliptical region that covers the main body of DEM L 192 and the north extension and a smaller square region that covers the southwest extension; these two regions together encompass all diffuse X-ray emission within the superbubble. The background contribution was assessed using an aperture exterior to DEM L 192 with similar area to the source aperture. All point sources were excised from the source and background apertures. A circular region that includes most stars in LH 54 is also excluded from the source aperture to minimize the stellar contribution to diffuse emission. After the background subtraction, a total of $\sim$16,000 counts are detected in the source aperture. Some residuals of the background subtraction are noticeable at the energy of the Al Kα fluoresce line at $\sim$1.5 keV. The energy range 1.45-1.55 keV, thus, has been omitted in the subsequent spectral analysis.

The background-subtracted EPIC/pn spectrum of DEM L 192, shown in Fig. 2, peaks at 0.5–0.6 keV, with a bright shoulder at $\sim$0.7 keV and a weaker peak at 0.9–1.0 keV. Above 1.0 keV, the spectrum is featureless with emission detected up to 3.5 keV. The overall spectral shape indicates thermal plasma emission, with spectral features corresponding to the He-like triplet of O VII at $\sim$0.57 keV, the H-like O VIII line at $\sim$0.65 keV, and the He-like triplet of Ne IX at $\sim$0.92 keV. Therefore, we have adopted the MEKAL optically-thin plasma emission model (Kaastra & Mewe 1993; Liedahl, Osterheld, & Goldstein 1995) with 1/3 $Z_{\odot}$ abundances as appropriate for the LMC and the absorption cross-sections from

Balucińska-Church & McCammon (1992). The spectral fits are carried out using XSPEC ver. 11.2.0 by folding the model spectrum through the EPIC/pn response matrices and comparing the modeled spectrum to the observed spectrum in the 0.3–4.5 keV energy range. The χ^2 statistics are used to determine the best-fit model.

The best-fit MEKAL model with 1/3 $Z_\odot$ abundances is very unsatisfactory (reduced χ^2 = 7.2), failing to fit the spectrum at 1–3 keV and showing large residuals at the Ne IX lines at ∼0.92 keV. Adding a second thermal component at a higher temperature can improve the spectral fits significantly (reduced $\chi^2 = 2.2$), but the temperature of the second component is pegged at the upper limit allowed by XSPEC, i.e., $kT = 80$ keV. A thermal component at such a high temperature is not expected in the ISM; furthermore, it is dominated by bremsstrahlung emission of which the spectral shape is featureless and similar to that of a power law. Therefore, we have added a power-law component, instead of a second thermal component, and the reduced χ^2 is lowered to 2.2 for the best-fit model. The large residuals at the Ne IX lines remain, and they can be minimized only if the Ne abundance is allowed to vary. By increasing the Ne abundance by a factor of 3 (i.e., solar Ne abundance and 1/3 solar for the other elements), we are able to obtain a best-fit model with a reduced χ^2 of 1.4, as shown in Fig. 2. This confirms the enhanced Ne abundance suggested by Bomans et al. (2002); however, we do not find compelling evidence for an enhanced O abundance, which has also been suggested by Bomans et al. (2002).

In our best-fit model for the diffuse X-rays from DEM L 192, the thermal component dominates the emission below 1 keV with a temperature kT of 0.21±0.01 keV, an absorption column density of (3.4±1.7)×10^{20} H-atom cm^{-2}, and a normalization factor[5] $A = (1.6\pm0.4)\times 10^{-3}$ cm^{-5}. The power law component dominates the emission from 1 to 3 keV and has a photon index Γ of 1.3 ± 0.2. The observed flux of diffuse X-ray emission from DEM L 192 is 1.1×10^{-12} ergs cm^{-2} s^{-1} and the X-ray luminosity is $\sim 4 \times 10^{35}$ ergs s^{-1} in the 0.3–3.0 keV band. The thermal emission accounts for ∼70% of the observed luminosity (but ∼85% of the total number of detected photons).

3. Energy Content of DEM L 192

For a superbubble like DEM L 192, we expect the stellar mechanical energy injected into the ISM to be stored in the thermal energy of its hot interior and the kinetic energy of the dense, swept-up shell. As the ionization front might be trapped in the swept-up shell, both

[5]The normalization factor A is defined to be A=$1 \times 10^{-14} \int N_{\rm e}^2 {\rm d}V/4\pi d^2$, where d is the distance, $N_{\rm e}$ is the electron number density, and V is the volume.

ionized and neutral gas in the superbubble shell must be considered. Below we examine separately the thermal energy of the hot interior and the kinetic energies of the ionized shell gas and associated H I gas.

3.1. Thermal Energy of the Superbubble Interior

The thermal energy of the hot gas in a superbubble is $E_{\rm th} = (3/2)kTN\epsilon_1 V$, where T is the plasma temperature, N is the total particle number density, ϵ_1 is the volume filling factor of the hot gas, and V is the volume interior to the superbubble. Assuming a canonical helium to hydrogen number density ratio of $N_{\rm He}/N_{\rm H} = 0.1$, the total particle number density, approximated by the sum of electron density, hydrogen density, and helium density, is $N \sim N_{\rm e} + N_{\rm H} + N_{\rm He} \sim 1.92N_{\rm e}$. For a given volume filling factor ϵ_1, the rms $N_{\rm e}$ can be derived from the normalization factor A of the best-fit model: $N_{\rm e} = 2 \times 10^7 d(\pi A/\epsilon_1 V)^{1/2}$. For a distance of $d = 50$ kpc, a normalization factor of $A = (1.4 \pm 0.4) \times 10^{-3}$ cm^{-5}, and a volume $V = 4.4 \times 10^{61}$ cm^3 (approximated by a $120 \times 120 \times 200$ pc^3 ellipsoid), we find $N_{\rm e} = (0.031 \pm 0.004)\ \epsilon_1^{-1/2}$ cm^{-3}. The total mass of the hot gas in the superbubble is $1.3 \times 10^3\ \epsilon_1^{1/2}$ M$_\odot$, and the total thermal energy of the hot gas is $E_{\rm th} = (1.3 \pm 0.3) \times 10^{51}\ \epsilon_1^{1/2}$ ergs. The filling factor ϵ_1 is most likely between 0.5 and 1.0. For $\epsilon_1 = 0.5$, $N_{\rm e} = 0.044 \pm 0.004$ cm^{-3}, the hot gas mass is 920 M$_\odot$, and $E_{\rm th} = (9 \pm 2) \times 10^{50}$ ergs.

The cooling timescale of the hot gas $t_{\rm cool}$ is $\sim (3/2)NkT/\Lambda(T)$, where $\Lambda(T)$ is the cooling function for gas at temperature T in units of ergs cm^{-3} s^{-1}. For a plasma temperature of a few $\times\ 10^6$ K, $\Lambda(T)/N_{\rm H}^2 = 7 \times 10^{-24}$ ergs cm^3 s^{-1} for 1/3 Z$_\odot$ abundances (Dalgarno & McCray 1972). With $N_{\rm H} \sim 0.83N_{\rm e}$, $N \sim 1.92N_{\rm e}$, and $kT = 0.21 \pm 0.01$ keV, the cooling timescale $t_{\rm cool}$ is ~ 200 Myr. Since the cooling timescale is much larger than the age of the OB associations LH 51 and LH 54, ~ 3 Myr, only a negligible amount of thermal energy has been radiated away.

3.2. Kinetic Energy of the Ionized Superbubble Shell

The mass of the ionized superbubble shell can be derived from the Hα luminosity, $L_{\rm H\alpha}$. The Hα flux from DEM L 192 is $f_{\rm H\alpha} = (860 \pm 80) \times 10^{-12}$ ergs s^{-1} cm^{-2} (Kennicutt & Hodge 1986). For a distance of $d = 50$ kpc, $L_{\rm H\alpha} = 4\pi d^2 f_{\rm H\alpha} = (2.6 \pm 0.3) \times 10^{38}$ ergs s^{-1}. In addition, for ionized gas at temperatures of $\sim 10^4$ K, $L_{\rm H\alpha} = 3.56 \times 10^{-25} N_{\rm e} N_{\rm p} V \epsilon_2$ ergs s^{-1}, where $N_{\rm e}$ and $N_{\rm p}$ are the particle number densities of electrons and protons in units of cm^{-3}, respectively, V is the volume of the region in units of cm^3, and ϵ_2 is the volume filling factor. Again, we

approximate the superbubble volume by a $120 \times 120 \times 200$ pc^3 ellipsoid, and the volume is $V = 4.4 \times 10^{61}$ cm^3. Helium is most likely singly ionized, thus $N_{\rm e} = 1.1 N_{\rm p} = (4.5 \pm 0.5)\ \epsilon_2^{-1/2}$ cm^{-3}. The total mass of the superbubble shell is $M = 1.27 N_{\rm e} V \epsilon_2 m_{\rm H}$, where $m_{\rm H}$ is the mass of a hydrogen atom. Using the rms $N_{\rm e}$ derived from $L_{\rm H\alpha}$, we find the superbubble shell mass to be $M = (4.2 \pm 0.5) \times 10^{38}\ \epsilon_2^{1/2}$ g $= (2.1 \pm 0.2) \times 10^5\ \epsilon_2^{1/2}$ M$_\odot$. The expansion velocity of the DEM L 192 superbubble has been measured in the Hα line to be $v_{\rm exp} \sim 35$ km s^{-1} (Meaburn & Terrett 1980). Thus, the kinetic energy in the ionized superbubble shell is $E_{\rm kin} = \frac{1}{2} M v_{\rm exp}^2$ $= (2.6 \pm 0.3) \times 10^{51} \epsilon_2^{1/2}$ ergs. If the thickness of the ionized superbubble shell is 1/10 of the radius, then the filling factor of shell gas is $\epsilon_2 = 0.27$, the ionized shell mass is $M \sim 1 \times 10^5$ M$_\odot$, and the ionized shell kinetic energy is $E_{\rm kin} \sim 1 \times 10^{51}$ ergs.

3.3. Kinetic Energy of Associated H I Gas

The kinetic energy of the neutral gas in the swept-up shell can be derived from observations of the 21-cm line emission from the H I gas. Such observations of DEM L 192 have been extracted from H I surveys of the LMC made with the Australia Telescope Compact Array (ATCA) and the Parkes Observatory 64-m telescope, where single-dish observations from the Parkes telescope have been combined with the ATCA data to "fill-in" low spatial frequencies not observed by the interferometer. The ATCA and Parkes observations are detailed in Kim et al. (1998) and Kim et al. (2003), respectively.

The kinematics of the H I gas can be determined from the position-velocity plots in Fig. 3. The H I gas shows a broad velocity profile centered at the systemic velocity of $V_{\rm hel} \sim 300$ km s^{-1} and with a width of $\sim$70 km s^{-1}, corresponding to twice the expansion velocity measured in Hα emission, but no clear expanding shell structure can be identified. The H I channel maps (Dunne, Chu, & Staveley-Smith 2004) and interstellar absorption observations of stars in DEM L 192 (Wakker et al. 2004) indicate that the H I velocity structure is rather complex and some velocity components may not be physically associated with the superbubble.

A total 21-cm line flux density of 470 Jy is measured from the combined radio observations within the dotted polygon outlined in the H I column density map in Fig. 3. Given the LMC distance of 50 kpc, we estimate a total H I mass of 3×10^5 M$_\odot$ from this flux density. The total kinetic energy of the H I gas can be approximated by 3/2 of the second moment of the integrated velocity profile, assuming that the motion is isotropic. This estimated kinetic energy is $\sim 3 \times 10^{51}$ ergs. We can also determine the H I kinetic energy using the total H I mass and the expansion velocity of the superbubble shell; the resulting kinetic energy is 3.7×10^{51} ergs, compatible with the H I kinetic energy estimated from the second moment

of the velocity profile. Note that these H I mass and kinetic energy estimates should be considered as upper limits, as some of the H I gas may not be physically associated with the superbubble.

4. Stellar Energy Injected into DEM L 192

Stellar mechanical energy is injected into the ambient ISM via fast stellar winds and supernova explosions. Below we determine the contributions of these two types of stellar energy feedback.

4.1. Stellar Wind Energy

To determine the stellar wind energy injected into DEM L 192, we consider the 50 most luminous stars in the OB associations LH 51 and LH 54 given by Oey & Smedley (1998). The spectroscopically determined spectral types of these stars are matched with the theoretical models of Schaerer & de Koter (1997) to assess the stellar mass M, mass loss rate $\dot{M}$, and stellar wind terminal velocity v_∞. Since $Z_{\rm LMC} \sim 1/3\ Z_\odot$, we apply the necessary corrections to the listed theoretical values of $\dot{M}$ and v_∞ for low metallicity stars as described in Schaerer & de Koter (1997). From these data, we estimate the stellar wind luminosity by $L_{\rm w} = (1/2)\dot{M}v_\infty^2$. The metallicity-corrected parameters and mechanical luminosities of the 50 stars are listed in Table 1 in the same order as given in Table 1 of Oey & Smedley (1998). We calculate the total mass loss rate to be 4.4×10^{-5} $M_\odot$ yr^{-1} and the total stellar wind luminosity to be 5.5×10^{37} ergs s^{-1}. Thus, for an age of ~ 3 Myr (Oey & Smedley 1998), the total stellar mass loss is ~ 100 $M_\odot$, and the total wind energy input is about $(5 \pm 1) \times 10^{51}$ ergs.

4.2. Supernova Energy

To estimate the number of stars that have already exploded as supernovae, we use the combined mass function of LH 51 and LH 54. UBV photometry of 456 stars in LH 51 and LH 54 is available from Oey (1996a). The mass of each main sequence star is determined by comparing its location on a color-magnitude diagram (CMD) to the evolutionary tracks of stars with different masses. As the reddening is not known for individual stars, we use the extinction-free magnitude $W = V - DM - (B-V)A_V/E(B-V)$ and reddening-free color $Q = (U-B) - (B-V)E(U-B)/E(B-V)$, where $DM = 18.5$ is the distance modulus of the

LMC, $E(U-B)/E(B-V) = 0.72$, and $A_V/E(B-V) = 3.1$. Fig. 4 shows the reddening-free CMD of LH 51 and LH 54, where the evolutionary tracks of main sequence stars with $Z = 0.4\ Z_\odot$ provided by Lejeune & Schaerer (2001) are plotted for initial masses of 5, 7, 10, 12, 15, 20, 25, 40, and 60 $M_\odot$. Stars in each mass bin are counted. We assume a Salpeter initial mass function for LH 51 and LH 54: $f(M) = KM^{-2.35}$, where K is a constant that can be determined from the star counts. The number of stars with masses between M_{min} and M_{max} is $N = \int_{M_{min}}^{M_{max}} f(M)\,dM$. For a M_{min} of 5–7 $M_\odot$ and a M_{max} of 20–25 $M_\odot$, we find K $= 3040 \pm 460$. This constant is insensitive to the choice of M_{max} but rather sensitive to the choice of M_{min}; the error bar reflects the uncertainty caused by different M_{min}. The number of stars with masses greater than 25 $M_\odot$ is $\int_{25M_\odot}^{100M_\odot} f(M)\,dM = 25 \pm 4$. From Table 1, we find 12 stars with masses greater than 25 $M_\odot$, so the number of stars that have exploded in supernovae is $(25 \pm 4) - 12 = 13 \pm 4$. We have chosen to count main-sequence stars in the 5–25 $M_\odot$ range because the evolutionary tracks of such stars are well constrained by the empirically derived relationship between stellar masses and spectral types and are not subject to the uncertainties for the most massive stars (e.g., Aloisi, Tosi, & Greggio 1999). We have compared the evolutionary tracks of stars in the 5–25 $M_\odot$ range between the Geneva models (Schaerer, Meynet, Maeder, & Schaller 1993) and the Padua models (Fagotto et al. 1994), and find that they are indeed similar. Assuming that each supernova releases about 10^{51} ergs of explosion energy, the total supernova energy input is approximately $(1.3 \pm 0.4) \times 10^{52}$ ergs.

5. Energy Budget of the Superbubble DEM L 192

The energies stored in the superbubble DEM L 192 and the stellar energy input are summarized in Table 2. The values and error bars of the thermal and kinetic energies take into account the most probable range of filling factors. The stellar energy input includes contributions from fast stellar winds and supernovae. The superbubble energy includes the thermal energy of its hot interior and the kinetic energy of the superbubble shell.[6] It is immediately clear that the expected amount of stellar energy injected into the ISM is ~ 3 times as large as that observed in the superbubble.

Previously, observed dynamics of bubbles blown by single stars or superbubbles have been compared with pressure-driven bubble models by Weaver et al. (1977) or variations of

[6]The thermal energy of the ionized superbubble shell is not included in the energy budget discussion because the superbubble shell is photoionized and the thermal energy is provided by the UV radiation of the OB associations.

such models, and it has been commonly concluded that the observed stellar wind strength is too high for the observed bubble dynamics or that the bubble/superbubble shell expands too slowly for the given stellar wind strengths (e.g., García-Segura, Langer, & Mac Low 1996; Oey 1996b; Nazé et al. 2001). These results are equivalent to what we have found in DEM L 192, i.e., the stellar mechanical energy injected into the ISM exceeds the energies storied in the superbubble. More specifically, according to the Weaver et al. (1977) model, the 35 km s^{-1} expansion velocity and 60 pc radius of DEM L 192 indicate a dynamic age of 1 Myr, which is shorter than the age of the OB associations LH 51 and LH 54. The mass of the ionized superbubble shell consists of the material swept up from the superbubble interior, thus the volume and mass of the H II gas given in §3.2 imply an ambient density of ~ 3 H-atom cm^{-3}. The wind mechanical luminosity required by Weaver et al. (1977) for DEM L 192 is 1.5×10^{38} ergs s^{-1}, and the total energy required during the 1 Myr dynamic time is $\sim 5 \times 10^{51}$ ergs, which is much smaller than the total stellar energy expected from LH 51 and LH 54.

Evidently there is an energy crisis: the observed interstellar energies cannot account for all the stellar energy injected into the ISM. Several mechanisms may drain energies from a superbubble. The most obvious mechanism is a superbubble blowout or breakout, in which the interior hot gas spews out, directly reducing the thermal energy and pressure of the superbubble interior. However, no blowouts are obvious in DEM L 192. As shown in Fig. 1, the extended diffuse X-ray emission from DEM L 192 is completely bounded by outer, curved Hα filaments, in sharp contrast to the blowout of the superbubble DEM L 152, also known as N44, in which the diffuse X-ray emission extends beyond open, streamer-like Hα filaments (Chu et al. 1993).

Another mechanism that may drain the internal energy of a superbubble is the evaporation of dense cooler gas into the hot interior. In addition to the dense ionized superbubble shell, DEM L 192 contains dense cloudlets with ionized surface layers, as revealed in high-resolution *HST* WFPC2 Hα images (Chen et al. 2000). The main energy loss would occur at the interface layer between the 10^6 K hot gas and the 10^4 K cool gas because the cooling rate is the highest for temperatures of a few $\times 10^5$ K. We may estimate the energy loss due to cooling from interface layers. Assuming that the interface layers are in pressure equilibrium with the hot interior gas, their electron number density would be 0.3–0.4 cm^{-3}. The total volume of the interface layers is nevertheless unknown because no interface layer has ever been spatially resolved observationally and even the existence of heat conduction and mass evaporation may be questionable (Shelton 2003). The spatial extent of an interface layer can be estimated from the relative locations of diffuse X-ray emission and the optical shell of a bubble or superbubble. The highest-quality X-ray observations of wind-blown bubbles are the *Chandra* observation of NGC 6888 and the *XMM-Newton* observations of S308 (Gruendl,

Guerrero, & Chu 2004; Chu et al. 2003). While NGC 6888 shows no appreciable separation between the outer edge of the diffuse X-ray emission and the outer edge of the optical shell, S308 shows a gap of 90–200″ (or 0.5 to 1.7 pc), which contains the dense ionized gas shell and the interface layer. The interface layer must be less than 0.5 pc in thickness. Adopting this upper limit of the interface layer thickness for DEM L 192, the volume occupied by the interface layer is no more than 2.5% of the total volume. Using a cooling function $\Lambda(10^5\mathrm{K})/N_\mathrm{H}^2 \sim 3 \times 10^{-22}$ ergs cm^3 s^{-1} appropriate for the LMC metallicity (Dalgarno & McCray 1972), the current cooling rate would be 4×10^{37} ergs s^{-1}. If the superbubble has been evolving with the radius $\propto t^\eta$, where t is the age and η is a constant (e.g., $\eta = 0.6$ for the Weaver et al. model), then the volume has been growing $\propto t^{3\eta}$, and the total energy radiated away in 3 Myr by the interface layer would be $4 \times 10^{51}(3\eta + 1)^{-1}$ ergs. If $\eta = 0.6$, the total radiative loss is $\sim 1.5 \times 10^{51}$ ergs. This generous upper limit for radiative loss is non-negligible but not sufficiently significant in the energy budget. Therefore, radiative loss in the interface layer between dense cold gas and the hot superbubble interior cannot be the cause of the energy discrepancy.

Where did the stellar energy go if it is not converted into the thermal and kinetic energies of the ISM? The interaction between a fast moving plasma, being it tenuous stellar winds or dense supernova ejecta, and the ambient ISM is a complex magnetohydrodynamic problem (Spitzer 1978). It is perhaps an oversimplification to assume that supernova ejecta and fast stellar winds are thermalized in the hot interior of a superbubble. In fact, the *XMM-Newton* X-ray observations of DEM L 192 reveal a possible mechanism that may play an important role in the energy budget. Our analysis of the X-ray spectrum of the diffuse emission from DEM L 192 indicates that not all emission originates from a thermal plasma; a power-law component is needed to explain the emission in the 1.0–3.0 keV range. This power-law component cannot originate from unresolved point sources, as the smoothed X-ray image in the 1.1–3.5 keV band displayed in Fig. 5 shows that this hard X-ray emission is diffuse. It is possible that this power-law component originates from the interactions of supernova ejecta and fast stellar winds with the hot interior of the superbubble, but the exact origin is unclear. It is unlikely that this power-law component represents a synchrotron X-ray emission similar to those seen in young supernova remnants such as SN 1006 (Koyama et al. 1995) and Cas A (Vink & Laming 2003) and the superbubble 30 Dor C (Bamba et al. 2004) for two reasons. First, the X-ray photon index of DEM L 192, $\Gamma = 1.3 \pm 0.2$, is lower than those observed in the other objects, $\Gamma \sim 2$. Second, the synchrotron X-ray emissions from young supernova remnants and 30 Dor C show limb-brightened morphologies because the relativistic particles are accelerated in the shocks, but the power-law X-ray emission from DEM L 192 does not show enhancement along the edge (see Fig. 5). Observations of more superbubbles are needed to determine whether a power-law component is commonly needed to model the spectra of

their diffuse X-ray emission. Future theoretical models of superbubbles need to solve the plasma interaction problem realistically instead of making simplifying assumptions about shocks and converting mechanical energy into only kinetic and thermal energies, so that true progress in the understanding of bubbles and superbubbles can be made.

YHC acknowledges the support of NASA grant NAG 5-13076. We thank the referee for prompt reading and providing useful suggestions to improve this paper. We also thank Yaël Nazé for her critical reading of the paper.

REFERENCES

Aloisi, A., Tosi, M., & Greggio, L. 1999, AJ, 118, 302

Balucińska-Church, M., & McCammon, D. 1992, ApJ, 400, 699

Bamba, A., Ueno, M., Nakajima, H., Koyama, K. 2004, ApJ, in press (astro-ph/0310713)

Bomans, D. J., Rossa, J., Weis, K., & Dennerl, K. 2002, in IAU Symposium, No. 212, ed. K. A. van der Hucht, A. Herrero, & C. Esteban (San Francisco: ASP), 637

Chen, C.-H. R., Chu, Y.-H., Gruendl, R. A., & Points, S. D. 2000, AJ, 119, 1317

Chu, Y.-H., Guerrero, M. A., Gruendl, R. A., García-Segura, G., & Wendker, H. J. 2003, ApJ, 599, 1189

Chu, Y.-H., & Mac Low, M.-M. 1990, ApJ, 365, 510

Chu, Y.-H., Mac Low, M. M., García-Segura, G., Wakker, B., & Kennicutt, R. C. 1993, ApJ, 414, 213

Dalgarno, A., & McCray, R. A. 1972, ARA&A, 10, 375

Davies, R. D., Elliott, K. H., & Meaburn, J. 1976, MmRAS, 81, 89

Dunne, B. C., Chu, Y.-H., & Staveley-Smith, L. 2004, in preparation

Dunne, B. C., Points, S. D., & Chu, Y. 2001, ApJS, 136, 119

Fagotto, F., Bressan, A., Bertelli, G., & Chiosi, C. 1994, A&AS, 105, 39

García-Segura, G., Langer, N., & Mac Low, M.-M. 1996, A&A, 316, 133

Gruendl, R. A., Guerrero, M. A., & Chu, Y.-H. 2004, in preparation

Henize, K. G. 1956, ApJS, 2, 315

Kaastra, J. S., & Mewe, R. 1993, Legacy, 3, 16, HEASARC, NASA

Kennicutt, R. C., Jr., & Hodge, P. W. 1986, ApJ, 306, 130

Kim, S., Staveley-Smith, L., Dopita, M.A., Freeman, K.C., Sault, R.J., Kesteven, M.J., & McConnell, D. 1998, ApJ, 503, 674

Kim, S., et al. 2003, ApJS, 148, 473

Koyama, K., Petre, R., Gotthelf, E. V., Hwang, U., Matsuura, M., Ozaki, M., & Holt, S. S. 1995, Nature, 378, 255

Lejeune, T., & Schaerer, D. 2001, A&A, 366, 538

Liedahl, D. A., Osterheld, A. L., & Goldstein, W. H. 1995, ApJ, 438, L115

Lucke, P. B., & Hodge, P. W. 1970, AJ, 75, 171

Mac Low, M., & McCray, R. 1988, ApJ, 324, 776

Meaburn, J., & Terrett, D. L. 1980, A&A, 89, 126

Nazé, Y., Chu, Y.-H., Points, S. D., Danforth, C. W., Rosado, M., & Chen, C.-H. R. 2001, AJ, 122, 921

Oey, M. S. 1996a, ApJS, 104, 71

Oey, M. S. 1996b, ApJ, 467, 666

Oey, M. S., & Smedley, S. A. 1998, AJ, 116, 1263

Salpeter, E. E. 1955, ApJ, 121, 161

Schaerer, D., & de Koter, A. 1997, A&A, 322, 598

Schaerer, D., Meynet, G., Maeder, A., & Schaller, G. 1993, A&AS, 98, 523

Shelton, R. L. 2003, ApJ, 589, 261

Spitzer, L., Jr. 1978, Physical Processes in the Interstellar Medium, (Wiley-Interscience)

Vink, J. & Laming, J. M. 2003, ApJ, 584, 758

Wakker, B. P., et al. 2004, in preparation

Weaver, R., McCray, R., Castor, J., Shapiro, P., & Moore, R. 1977, ApJ, 218, 377

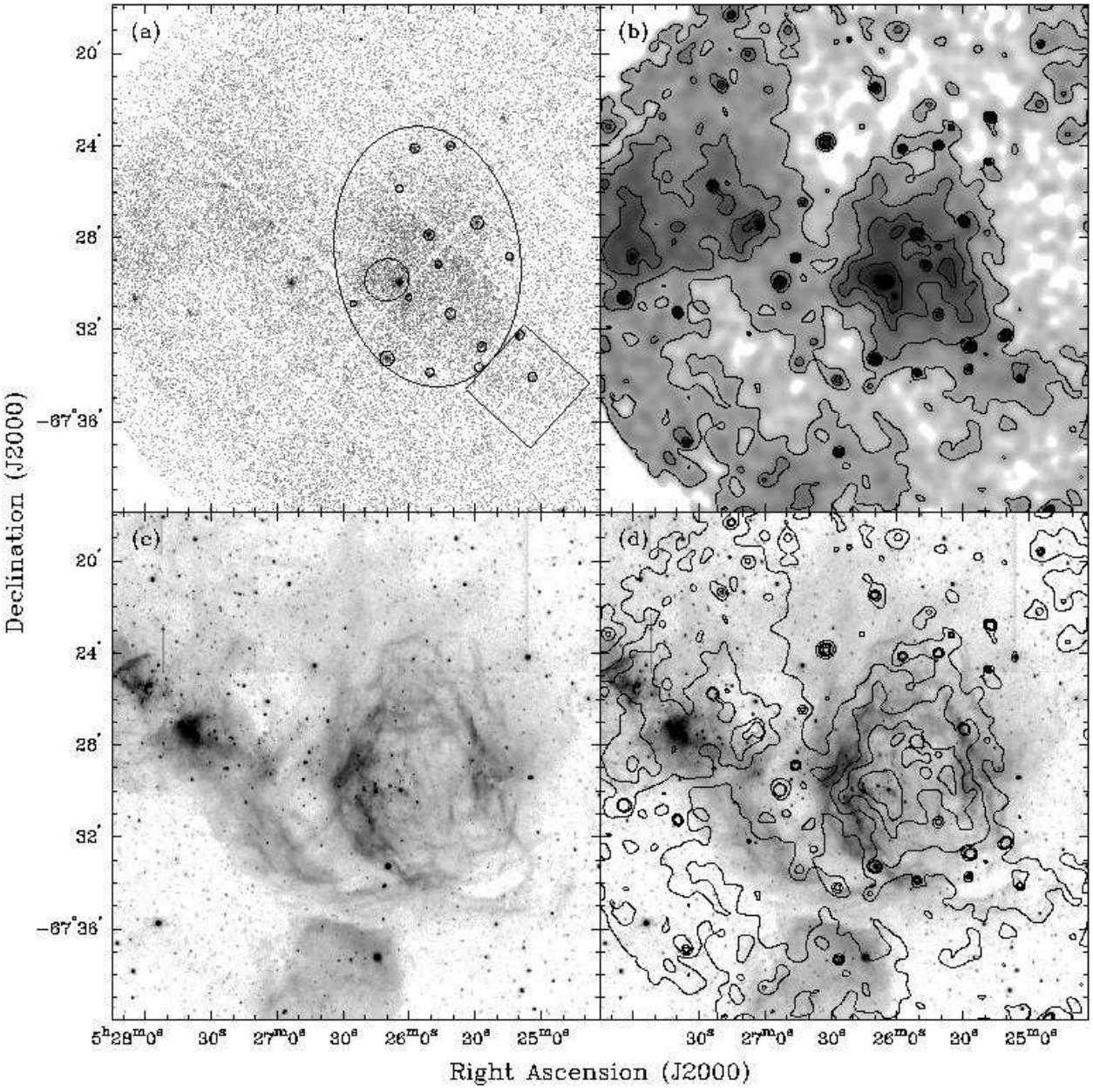

Fig. 1.— (a) *XMM-Newton* EPIC image of DEM L 192. The spectrum of the diffuse X-ray emission is extracted from the source aperture consisting of elliptical and square regions marked. The point sources, marked by small circles, and stellar emission from the OB association LH 54, marked by a larger circle, are excluded from the source aperture. (b) Adaptively smoothed and vignetting-corrected X-ray image. The contour levels are at 9, 15, 22.5, and 30 σ above the background. (c) Hα image of DEM L 192. (d) Hα image overplotted with X-ray contours.

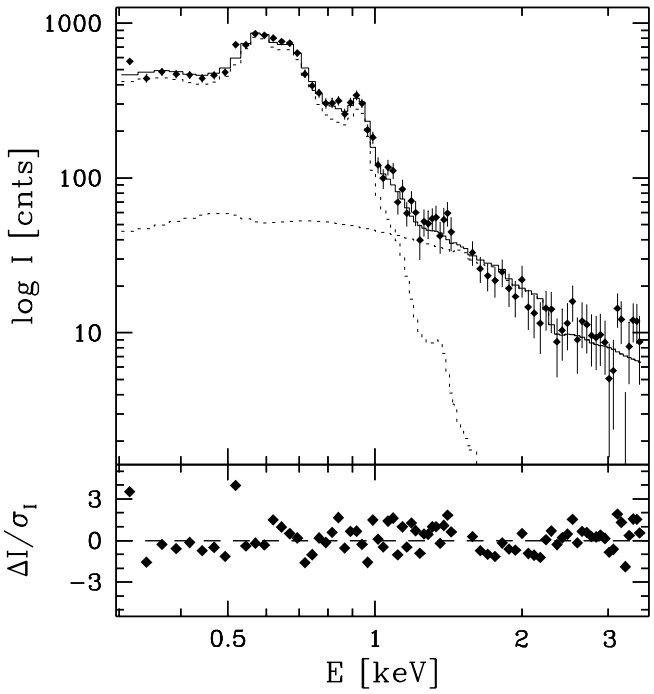

Fig. 2.— *XMM-Newton* EPIC/pn spectrum of the diffuse X-ray emission from DEM L 192. The best-fit model is overplotted in the solid curve. The thermal plasma component and the power-law component are individually plotted in dashed curves. The bottom panel plots the residuals of the fit.

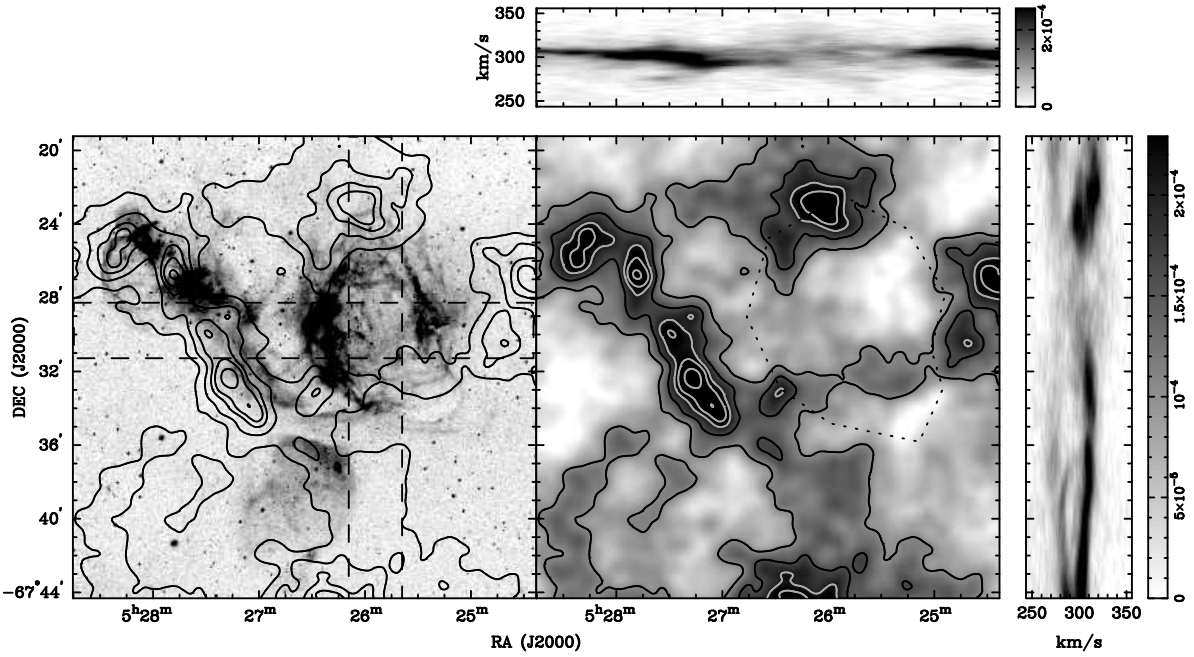

Fig. 3.— Hα image (left) and H I 21-cm line map (right) of DEM L 192. Both images are overlaid with H I 21-cm line emission contours at levels of 50%, 65%, 77%, 85%, and 95% of the peak. The dotted polygon plotted over the H I map represents the extent of the superbubble and the region over which the H I mass is extracted. We have produced position-velocity plots for two 3′-wide slices through the superbubble along the right ascension and declination axes. These slices are shown above and to the right, respectively, of the H I image accompanied with greyscale wedges in arbitrary units. The velocities are heliocentric. The area covered by each slice is indicated by the dashed lines on the Hα image.

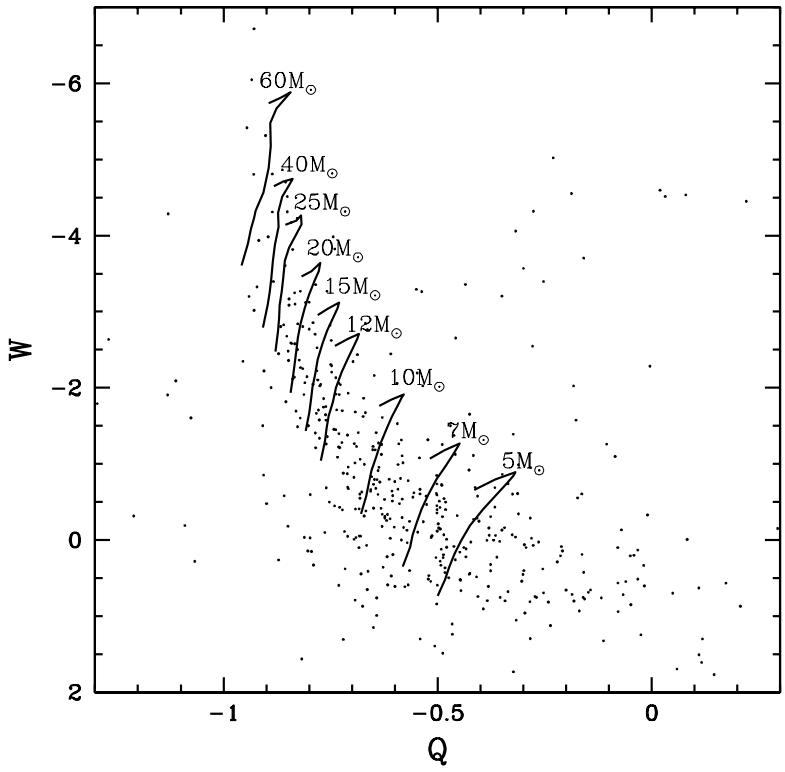

Fig. 4.— Reddening-free color-magnitude diagram of stars in LH 51 and LH 54. The photometric data of these 456 stars are from Oey (1996a). See the text for the definition of the reddening-free magnitude W and color Q. The evolutionary tracks of stars are from Lejeune & Schaerer (2001).

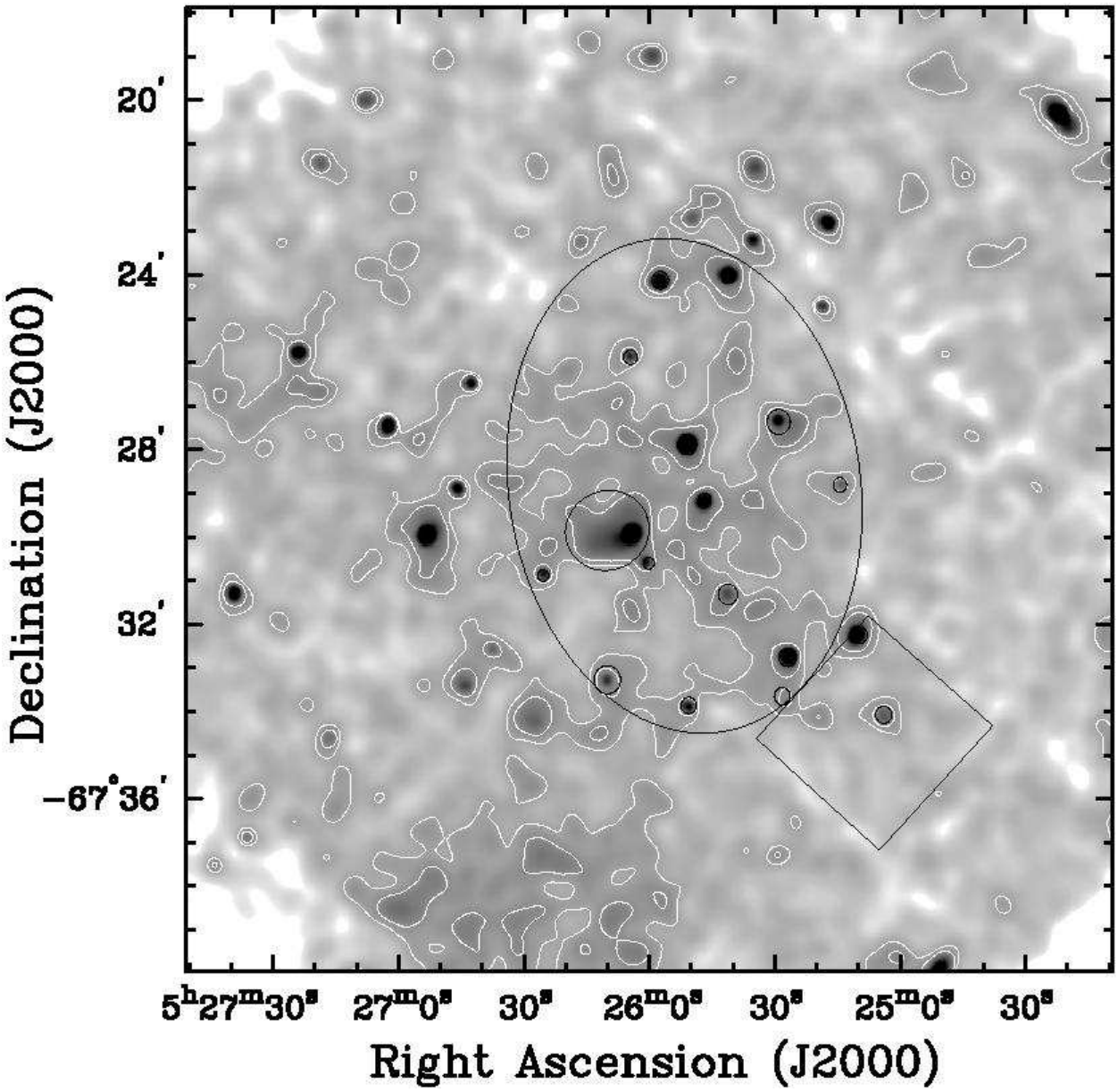

Fig. 5.— *XMM-Newton* pn image of DEM L 192 in the 1.1–3.5 keV energy band. The image has been adaptively smoothed with Gaussians of FWHM of 2″ to 15″. The emission in the 1.1–3.5 keV range is dominated by the power-law component. The contours are at 3σ and 6σ above the background. It is evident that the diffuse emission in this energy range is widespread. The source regions are marked for comparison with Fig. 1a.

Table 1. Stellar Data

Star ID	Spectral Type	M ($M_\odot$)	$\log \dot{M}$ ($M_\odot$ yr^{-1})	v_∞ (km s^{-1})	$\log L_{\rm w}$ (ergs s^{-1})
L54SA-1b	O8 Iaf	51	-5.170	1699	36.79
L54SA-2	O8 III((f))	55	-5.491	2064	36.64
L54S-2	O9 Ib(f)	51	-5.170	1699	36.79
L51N-1	O8.5 III((f))	55	-5.491	2064	36.64
L54S-1a	O7: III(f)	55	-5.491	2064	36.64
L54S-4	O4 III(f*)	96	-5.105	2445	37.17
L54S-5	O8 III((f))	55	-5.491	2064	36.64
L54S-3a	O6.5: V	32	-6.527	2422	35.54
L54S-3b	B2: II:	19	-6.623	1561	35.26
L54S-1b	B0.5: III:	19	-6.623	1561	35.26
L54N-2	O6.5 V	32	-6.527	2422	35.54
L54N-3	B1 IIIe	19	-6.623	1561	35.26
L54N-4	O9 V	20	-7.096	2205	35.09
L54S-8	B0.5 Ib	34	-5.529	1438	36.29
L51N-3	O9 V	20	-7.096	2205	35.09
L54S-9	B0 III	19	-6.623	1561	35.26
L54N-6	O9 V	20	-7.096	2205	35.09
L54S-10	early B:: +neb	19	-6.873	1909	35.19
L54N-7	B0.5:: V +neb	19	-6.873	1909	35.19
L51S-2	O6 V((f))e	39	-6.409	2332	35.83
L54SA-4	B0.5 III	19	-6.623	1561	35.26
L54S-12	B0 V #	19	-6.873	1909	35.19
L54S-13	B0.5 Ve	19	-6.873	1909	35.19
L54S-14	O9.5 V	20	-7.096	2205	35.09
L54S-15	O8 Ve	24	-6.835	2244	35.37
L54S-16	O9.5 V #	20	-7.096	2205	35.09
L51S-3	O8 V	24	-6.835	2244	35.37
L51S-4	B0.5 V	19	-6.873	1909	35.19
L54S-18	O9 V	20	-7.096	2205	35.09
L54S-19	B0.5: V #	19	-6.873	1909	35.19

Table 1—Continued

Star ID	Spectral Type	M ($M_\odot$)	$\log \dot{M}$ ($M_\odot$ yr^{-1})	v_∞ (km s^{-1})	$\log L_w$ (ergs s^{-1})
L51S-5	B0.5 V	19	-6.873	1909	35.19
L51N-9	B1: V +neb	19	-6.873	1909	35.19
L51N-10	B0 V	19	-6.873	1909	35.19
L54S-20	O9.5 V	20	-7.096	2205	35.09
L54SA-5	B1:: V +neb	19	-6.873	1909	35.19
L51S-7	O9.5 V	20	-7.096	2205	35.09
L54SA-1a	WC 5	...	...	...	...
L51N-12	B0.5 V +neb	19	-6.873	1909	35.19
L54S-22	O9.5-B0 V	19	-6.873	1909	35.19
L54S-24	O9.5 V +neb	20	-7.096	2205	35.09
L54N-14	O9.5 V	20	-7.096	2205	35.09
L54S-25	B1.5 III +neb	19	-6.873	1909	35.19
L54N-16	O9.5 V	20	-7.096	2205	35.09
L54S-26	B1:: V +neb	19	-6.873	1909	35.19
L54N-18	O6: Ve	39	-6.409	2332	35.83
L51S-9	B0:: V	19	-6.873	1909	35.19
L54SA-7	B1.5 V	19	-6.873	1909	35.19
L54N-19	O9.5 V	20	-7.096	2205	35.09
L54N-21	B2.5 V	19	-6.873	1909	35.19
L54S-36	B1.5:: Ve	19	-6.873	1909	35.19
L54N-25	B2:: V +neb	19	-6.873	1909	35.19
L54N-27	O9.5-early Be	19	-6.873	1909	35.19
L51S-14	B1:: V	19	-6.873	1909	35.19
L54N-33	B1:: V	19	-6.873	1909	35.19

Note. — # indicates spectral binary candidate. See Table 1 of Oey & Smedley (1998)

Table 2. Energy Budget of the Superbubble DEM L 192

Energies	Amount ($\times 10^{51}$ ergs)
$E_{\rm th}$ of the hot gas in superbubble interior	1.1 ± 0.5
$E_{\rm kin}$ of the ionized (H II) superbubble shell	1.5 ± 0.5
$E_{\rm kin}$ of the neutral (H I) superbubble shell	3.2 ± 0.5
Total energy observed in the superbubble	6 ± 2
Stellar wind energy input in 3 Myr	5 ± 1
Supernova energy input	13 ± 4
Total stellar energy input	18 ± 5